Electronic Supplementary Information (ESI) for New Journal of Chemistry

Supporting Information

Facile synthesis of FeCo alloys encapsulated in nitrogen-doped graphite/carbon nanotube hybrids: efficient bi-functional electrocatalysts for oxygen and hydrogen evolution reactions

Bing Du,[a] Qing-Ting Meng,[a] Jing-Quan Sha,[a]* and Ji-Sen Li[a,b]*

[a]Key Laboratory of Inorganic Chemistry in Universities of Shandong, Department of Chemistry and Chemical Engineering, Jining University, Qufu, Shandong 273155, China

[b]College of Chemistry, Chemical Engineering and Materials Science, Collaborative Innovation Center of Functionalized Probes for Chemical Imaging in Universities of Shandong, Key Laboratory of Molecular and Nano Probes, Ministry of Education, Shandong Provincial Key Laboratory of Clean Production of Fine Chemicals, Shandong Normal University, Shandong 250014, China

*E-mail: senjili@sina.com

S1. Figures in Supporting Information

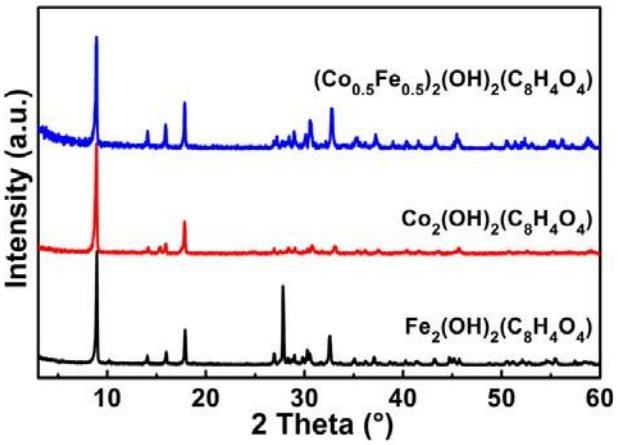

Fig. S1 PXRD patterns of the as-synthesized of $Fe_2(OH)_2(C_8H_4O_4)$, $Co_2(OH)_2(C_8H_4O_4)$, and $(Co_{0.5}Fe_{0.5})(OH)_2(C_8H_4O_4)$, respectively.

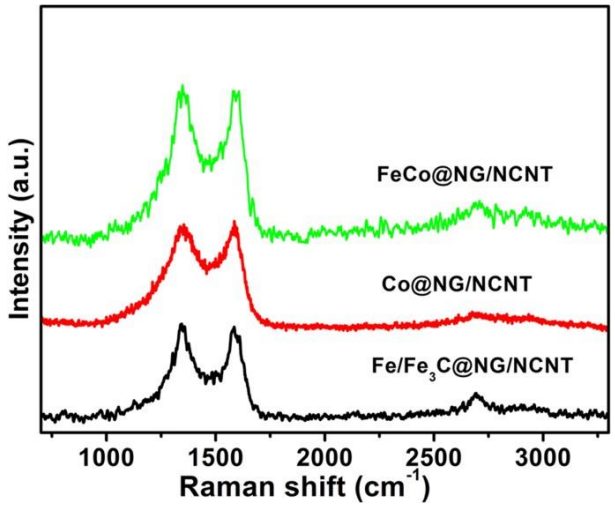

Fig. S2 Raman spectra of Fe/Fe_3C@NG/NCNT, Co@NG/NCNT, and FeCo@NG/NCNT, respectively.

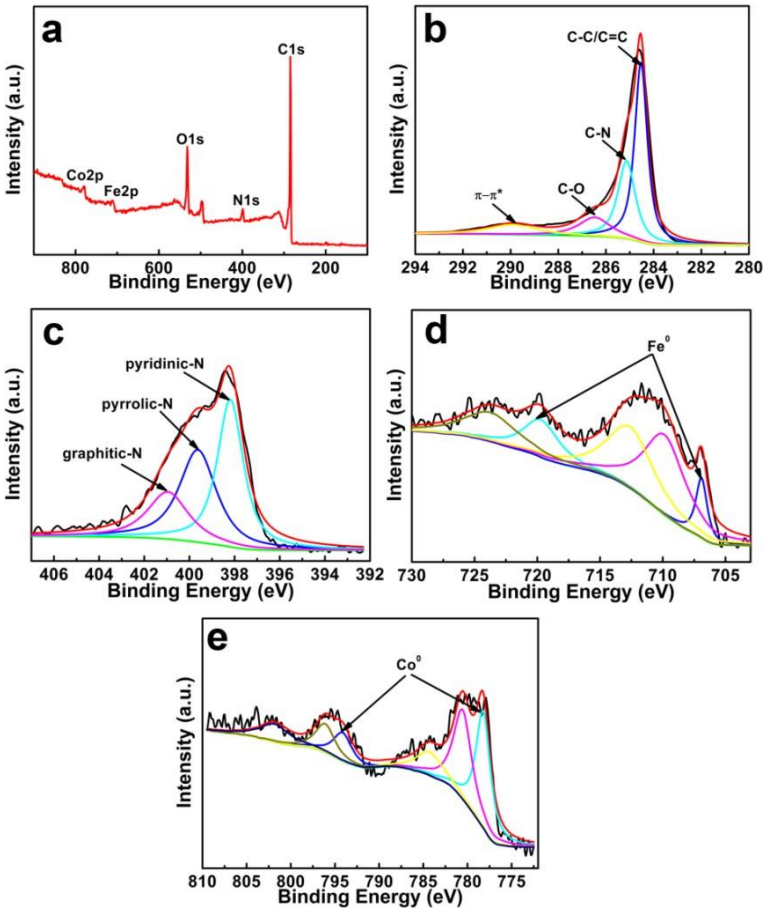

Fig. S3 XPS survey spectra (a) and high-resolution XPS spectra of (b) C 1s, (c) N 1s, (d) Fe 2p, and (e) Co 2p of FeCo@NG/NCNT.

The chemical compositions and valence states of the obtained sample were investigated by X-ray photoelectron spectra (XPS), as shown in **Fig. S3**. The XPS survey spectrum dislays the hybrid is composed of C, N, Fe, Co, O (**Fig. S3a)**. The C1s XPS spectrum shown in **Fig. S3b** reveals four peaks at 284.5, 285.1, 286.5, and 289.9 eV, assigned to C-C/C=C, C-N, C-O, and π-π* satellite, respectively. The deconvolution of N1s energy level signals exhibit three peaks at 398.1, 399.2, and 400.4 eV (**Fig. S3c**), which are ascribed to pyridinic-N, pyrrolic-N, and graphitic-N, respectively. Generally, pyridinic-N, and graphitic-N is beneficial to boosting catalytic activity. As presented in **Fig. S3d**, the two peaks at 706.9 and 719.7 eV should be ascribed to metallic Fe $2p_{3/2}$ and Fe $2p_{1/2}$, respectively. As well, the high resolution Co 2p XPS exhibits two peaks at 778.2 and 793.9 eV (**Fig. S3e**), corresponding to metallic Co. Noticeably, it was found that oxidation states of Fe and Co are also detected due to the surface oxidation when exposed to air.

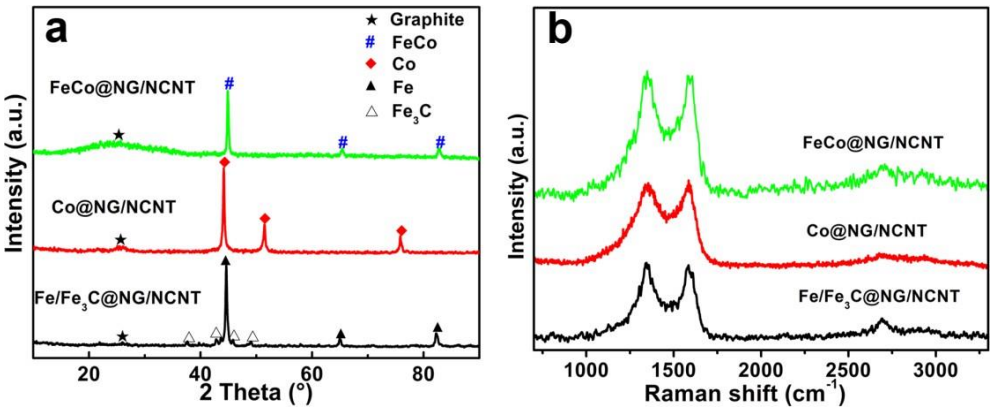

Fig. S4 PXRD patterns and Raman spectra of Fe/Fe_3C@NG/NCNT, Co@NG/NCNT, and FeCo@NG/NCNT, respectively.

For Co@NG/CNT, it is clearly seen that the characteristic peaks of (111) at 44.2^o, (200) at 51.5^o, and (220) at 75.8^o, which are well matched with the Co phase (JCPDS, No, 89-4307) (**Fig. S4**). For Fe/Fe_3C@NG/NCNT, the three distinct peaks located around 44.7^o, 64.9^o, and 82.2^o belong to the (110), (200), and (211) planes of a cubic Fe phase (JCPDS, No, 89-7194) (**Fig. S4**). Besides, an amount of Fe_3C (JCPDS, No, 89-2867) is also detected.

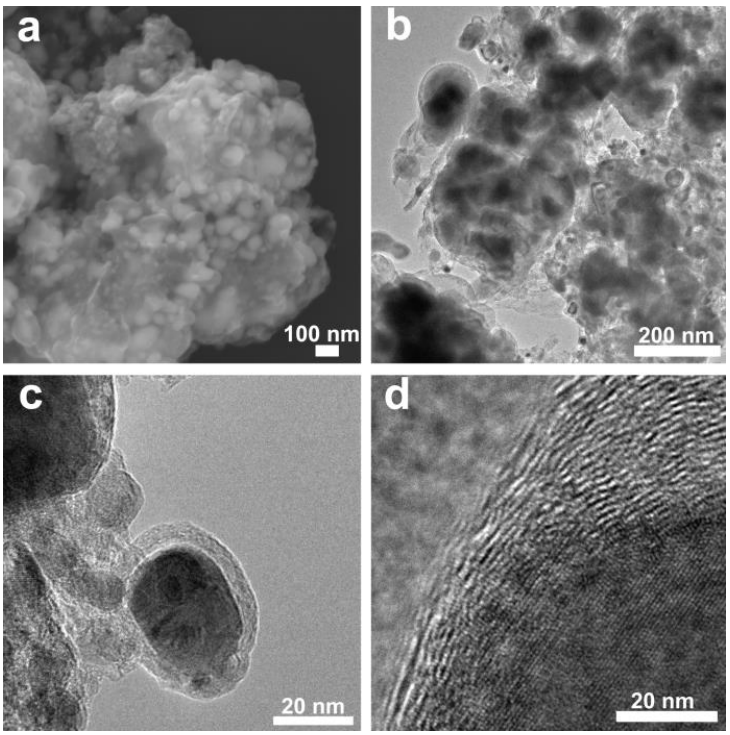

Fig. S5 (a) SEM, (b-c) TEM, and (d) HRTEM images of Fe/Fe_3C@NG/NCNT.

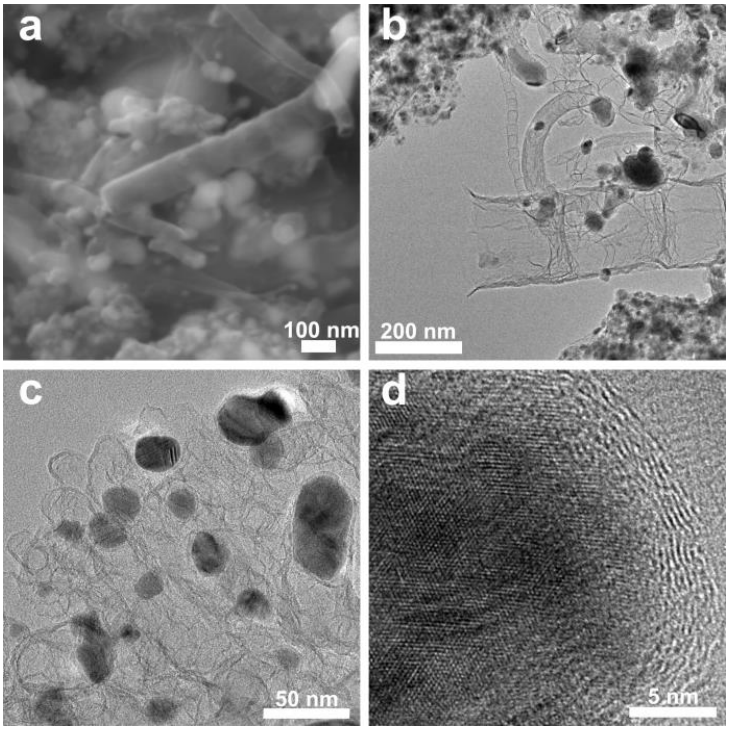

Fig. S6 (a) SEM, (b-c) TEM, and (d) HRTEM images of Co@NG/NCNT.

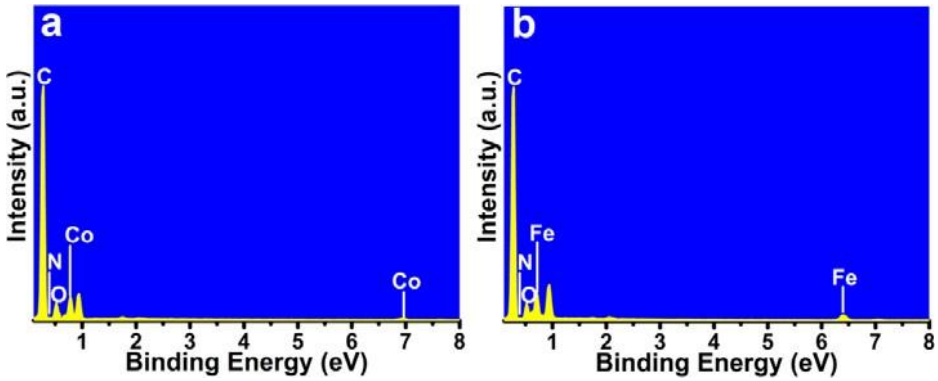

Fig. S7 (a-b) EDX of Co@NG/NCNT, and Fe/Fe_3C@NG/NCNT, respectively.

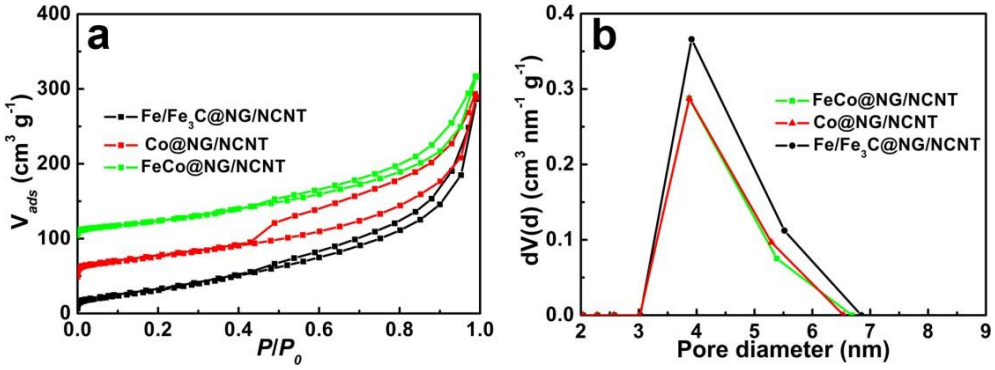

Fig. S8 (a) N_2 adsorption-desorption isotherms and (b) the corresponding pore size distribution of FeCo@NG/NCNT, Fe/Fe_3C@NG/NCNT, and Co@NG/NCNT. For clarity, isotherms of Co@NG/NCNT , and FeCo@NG/NCNT are offset by 40, and 100 cm^3 g^{-1}.

N_2 adsorption-desorption isotherms were adopted to examine the specific surface area and pore size of these samples (**Fig. S8**). The Brunauer-Emmett-Teller (BET) surface area of Fe/Fe_3C@NG/NCNT, and Co@NG/NCNT were determined to be 102.7, and 105.1 m^2 g^{-1}, respectively. The corresponding pore size distribution is centered at about 4 nm by Barrett-Joyner-Halenda (BJH) method, suggesting the presence of mesoporous structure.

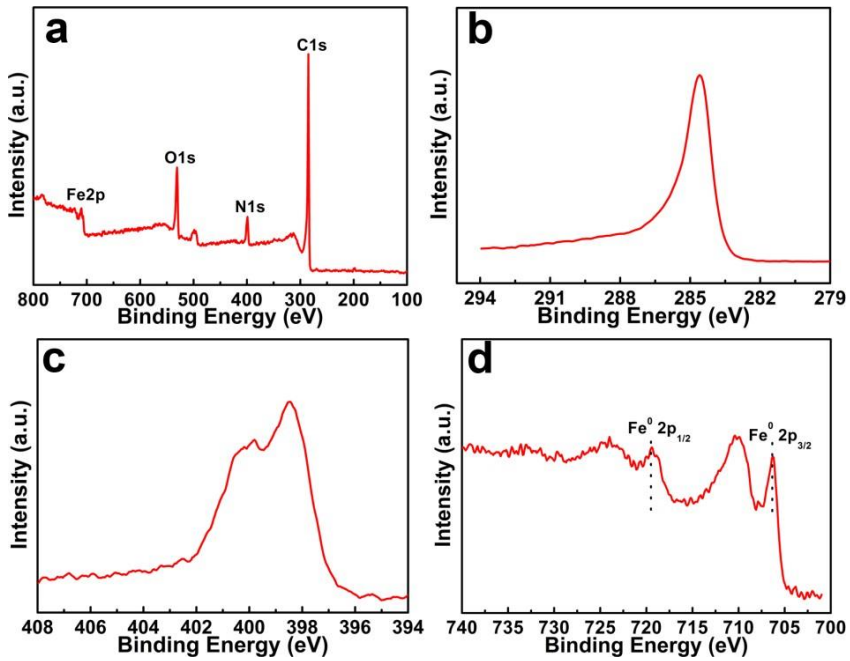

Fig. S9 (a) XPS survey spectrum and high resolution XPS spectra of (b) C 1s, (c) N 1s, and (d) Fe 2p of Fe/Fe_3C@NG/NCNT, respectively.

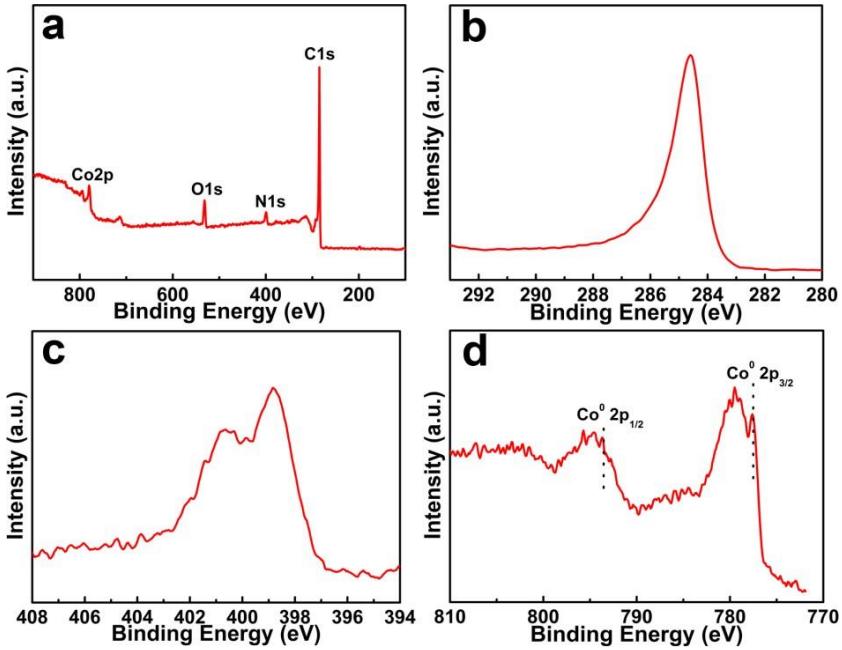

Fig. S10 (a) XPS survey spectrum and high resolution XPS spectra of (b) C 1s, (c) N 1s, and (d) Co 2p of Co@NG/NCNT, respectively.

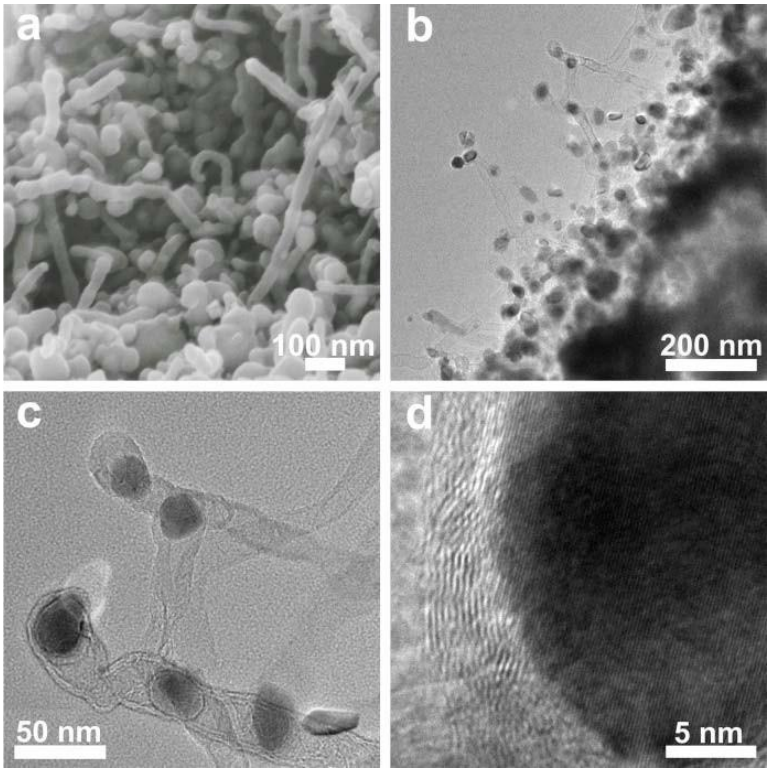

Fig. S11 (a) SEM, (b-c) TEM, and (d) HRTEM images of FeCo@NG/NCNT-800.

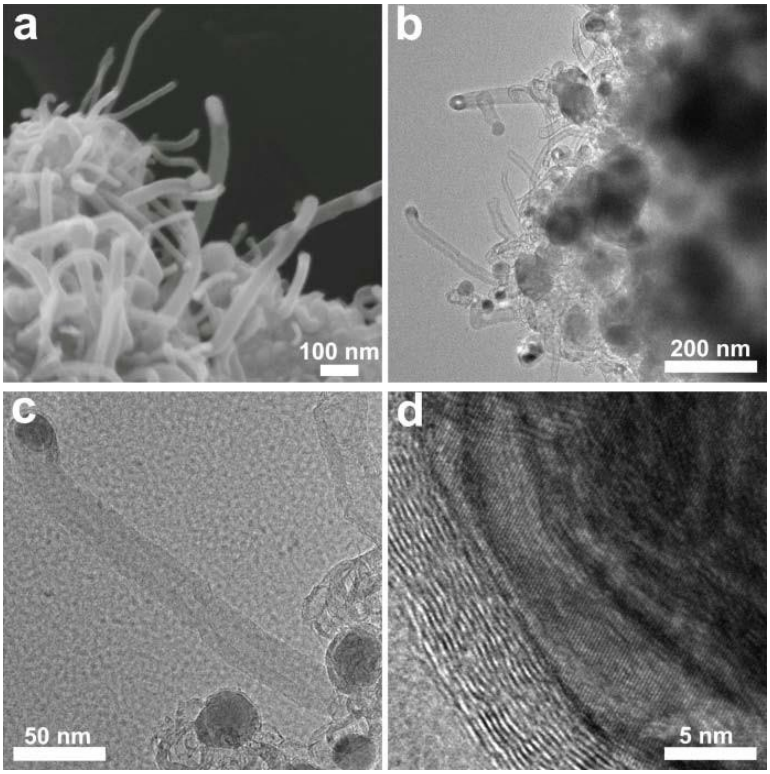

Fig. S12 (a) SEM, (b-c) TEM, and (d) HRTEM images of FeCo@NG/NCNT-1000.

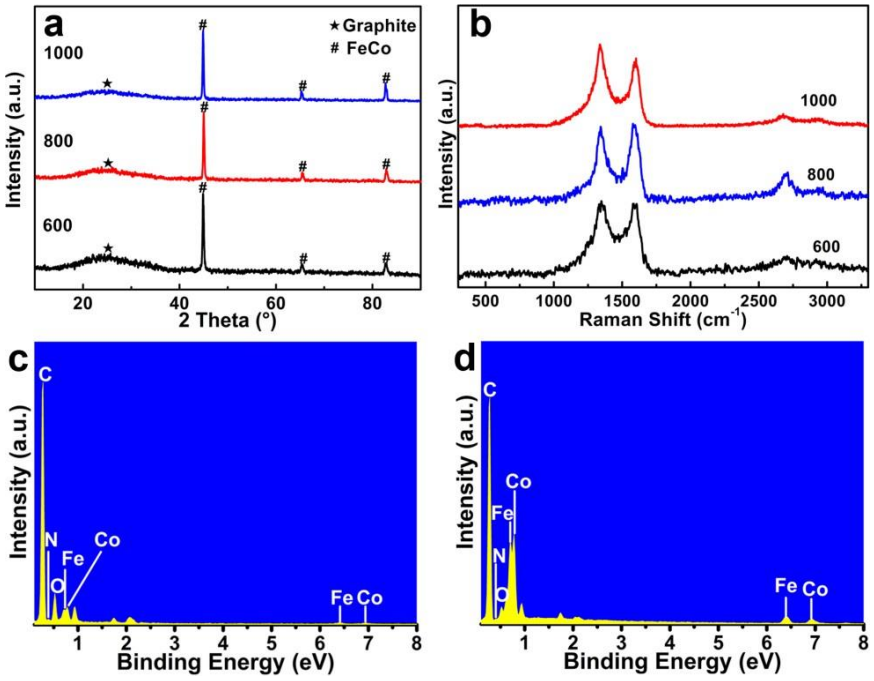

Fig. S13 (a-b) PXRD patterns and Raman spectra of FeCo@NG/NCNT carbonized at 600, 800, and 1000 ^{o}C, respectively. (c-d) EDS of FeCo@NG/NCNT carbonized at 800, and 1000 ^{o}C, respectively.

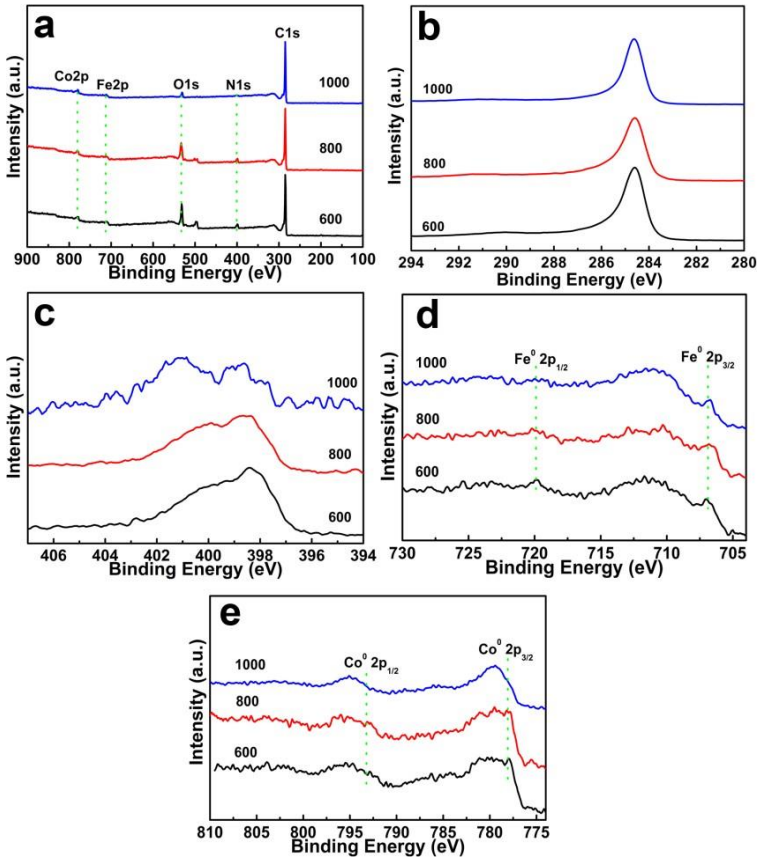

Fig. S14 XPS survey spectra (a) and high-resolution XPS spectra of (b) C 1s, (c) N 1s, (d) Fe 2p, and (e) Co 2p of FeCo@NG/NCNT carbonized at 600, 800, and 1000 ^{o}C, respectively.

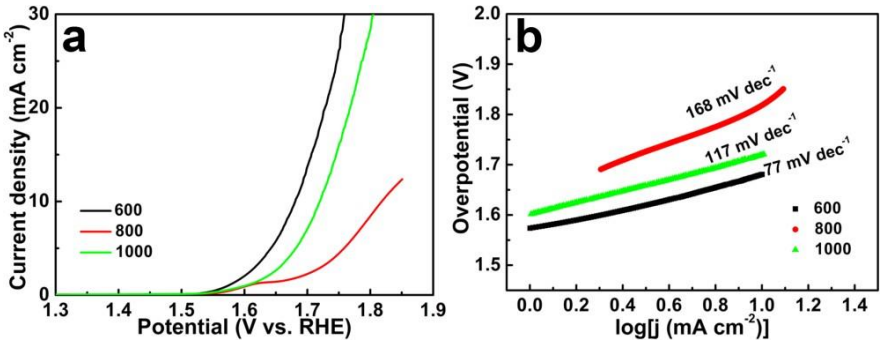

Fig. S15 (a) OER polarization curves of FeCo@NG/NCNT carbonized at 600, 800, and 1000 ^{o}C, respectively. (b) Corresponding Tafel plots of a.

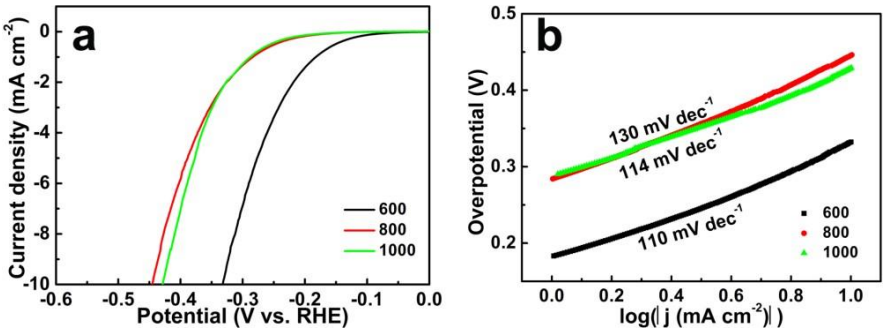

Fig. S16 (a) HER polarization curves of FeCo@NG/NCNT carbonized at 600, 800, and 1000 ^{o}C, respectively. (b) Corresponding Tafel plots of a.

S2. Tables in Supporting Information

Table S1. Elemental compositions of the catalysts determined by ICP, respectively.

Materials	Elemental composition (at %)	
	Fe_{2p}	Co_{2p}
FeCo@NG/NCNT	1.65	1.46
Fe/Fe_3C@NG/NCNT	3.03	0
Co@NG/NCNT	0	3.64
FeCo@NG/NCN-800	1.42	1.35
FeCo@NG/NCN-1000	1.72	1.83

Table S2. Elemental compositions of these catalysts determined by XPS, respectively.

Materials	Elemental composition (at %)				
	C_{1s}	N_{1s}	Fe_{2p}	Co_{2p}	O_{1s}
FeCo@NG/NCNT	78.96	5.21	1.22	1.19	13.42
Fe/Fe_3C@NG/NCNT	76.26	9.3	2.54	0	11.9
Co@NG/NCNT	80.78	6.85	0	3.22	9.15
FeCo@NG/NCN-800	81.4	3.22	1.12	1.02	13.24
FeCo@NG/NCN-1000	90.95	1.35	1.34	1.45	4.91

Table S3. Comparison of OER performance in basic media for FeCo@NG/NCNT with other non-noble metal electrocatalysts.

Catalyst	Onset potential [mV][a]	Tafel slope [mV dec^{-1}]	η_{10} [mV][a]	Reference
FeCo@NG/NCNT	1.54	77	450	This work
Co_3O_4-MTA	1.52	84	--	*Angew. Chem. Int. Ed.*, 2017, **56**, 1324-1328
Ni@NC-800	1.45	45	280	*Adv. Mater.*, 2017, **29**, 1605957
NiCo/PFC	--	106	400	*Nano Lett.*, 2016, **16**, 6516-6522
$FeNi_3N$/Ni foam	1.43	40	202	*Chem. Mater.*, 2016, **28**, 6934-6941
Co@NCNTs	--	128	410	*J. Power Source*, 2017, **338**, 26-33
NPCN/CoNi-NCNT	1.57	165	360	*Small*, 2015, **11**, 5940-5948
Porous Ni-P foam	--	179.9	332	*J.Mater. Chem. A*, 2016, **4**, 5639-5646
Ni-P	1.48	64	330	*Energy Environ. Sci.*, 2016, **9**, 1246-1250
Co_3O_4 NCs	1.52	101	---	*Chem. Commun.*, 2015, **51**, 8066-8069

[a] represents the overpotential (η) at the current density of 10 mA cm^{-2}. The potential measured versus RHE.

Table S4. Comparison of HER performance in basic media for FeCo@NG/NCNT with other non-noble metal electrocatalysts.

Catalyst	Onset overpotential [mV][a]	Tafel slope [mV dec^{-1}]	η_{10} [mV][a]	Reference
FeCo@NG/NCNT	75	110	332	This work
Ni@NC-800	105	160	205	*Adv. Mater.*, 2017, **29**, 1605957
Co_3O_4-MTA	100	98	--	*Angew. Chem. Int. Ed.*, 2017, **56**, 1324-1328
FeCo	--	77	211	*ACS Catal.*, 2017, **7**, 469-479.
FeNi3N/Ni foam	--	98	75	*Chem. Mater.*, 2016, **28**, 6934-6941
MnNi	150	--	360	*Adv. Funct. Mater.*, 2015, **25**, 393-399.
NiSe/NF	--	120	96	*Angew. Chem. Int. Ed.*, 2015, 54, 9351-9355
Co_3O_4 NCs	50	116	380	*Chem. Commun.*, 2015, **51**, 8066-8069.
Co-NRCNTs	--	--	370	*Angew. Chem. Int. Ed.*, 2014, **53**, 4372-4376
N-Co@G	70	--	337	*ACS Appl. Mater. Interfaces*, 2015, **7**, 8083-8087
Co@Co-N-C	78	59	314	*Chem. Commun.*, 2015, **51**, 8942-8945

[a] represents the overpotential (η) at the current density of 10 mA cm^{-2}. The potential measured versus RHE.